Braz J Phys (2017) 47:461–472
DOI 10.1007/s13538-017-0510-3

SOCIEDADE BRASILEIRA DE FÍSICA

NUCLEAR PHYSICS

# Role of Barrier Modification and Nuclear Structure Effects in Sub-Barrier Fusion Dynamics of Various Heavy Ion Fusion Reactions

**Manjeet Singh Gautam**[1] · **K. Vinod**[1] · **Hitender Kumar**[2]

Received: 24 March 2017 / Published online: 1 August 2017


**Abstract** The role of barrier modifications and the relevant nuclear structure effects in the fusion of the ${}^{16}_{8}O + {}^{144,148,150,152,154}_{62}Sm$ and ${}^{6,7}_{3}Li + {}^{152}_{62}Sm$ systems is analyzed within the context of the energy-dependent Woods-Saxon potential model (EDWSP model) and the coupled channel model. For the ${}^{16}_{8}O + {}^{144,148,150,152,154}_{62}Sm$ reactions, where the colliding pairs are stable against breakup, the collective excitations and/or static deformations are sufficient to account for the observed fusion enhancement. In contrast, the model calculations overpredict the complete fusion data at above - barrier energies for the ${}^{6,7}_{3}Li + {}^{152}_{62}Sm$ systems, where the importance of projectile breakup effects has been pointed out. Due to the low threshold of the *alpha*-breakup channel, the weakly bound projectiles $\left({}^{6,7}_{3}Li\right)$ break up into charged fragments before reaching the fusion barrier and consequently the complete fusion cross section is suppressed by 28% (25%) in the ${}^{6}_{3}Li + {}^{152}_{62}Sm\left({}^{7}_{3}Li + {}^{152}_{62}Sm\right)$ reaction with respect to predictions of coupled channel calculations. However, the EDWSP model based calculations can minimize the suppression factor by as much as of 13% (8%) in the ${}^{6}_{3}Li + {}^{152}_{62}Sm\left({}^{7}_{3}Li + {}^{152}_{62}Sm\right)$ reaction with reference to the predictions made by the coupled channel calculations. Therefore, the complete fusion data of the ${}^{6}_{3}Li + {}^{152}_{62}Sm\left({}^{7}_{3}Li + {}^{152}_{62}Sm\right)$ reaction at above - barrier energies is reduced by 15% (17%) with respect to the expectations of the EDWSP model. The extracted suppression factors for the studied reactions are due to the modifications of the barrier profile as a consequence of the energy - dependence in nucleus-nucleus potential, and thus greater barrier modifications occur for more weakly bound system, which in turn, confirms the breakup of projectile in the incoming channel.

**Keywords** Woods-Saxon potential · Heavy-ion near-barrier fusion reactions · Coupled channel equations · Weakly bound nuclei

## 1 Introduction

The dynamics of heavy ion fusion reactions attracts researchers not only for stellar energy production and nucleosynthesis in stars but also for providing good insight about nuclear structure and related aspects of the participating nuclei. In the fusion process, the projectile and target interact with each other via repulsive Coulomb interaction and short-range attractive nuclear interactions, and form a compound nucleus either by overcoming or by quantum tunneling through the fusion barrier [1–8]. The substantially large enhancement observed in measured fusion cross sections over the expectations of the one-dimensional barrier penetration model for many projectile-target combinations points toward the involvement of nuclear structure effects associated with the colliding systems. Recent experimental and theoretical investigations revealed that such fusion enhancement has an intimate link with the collective excitations and/or static deformations of the colliding nuclei [9–11]. In heavy ion reactions, one of the familiar problems is to decide which of the various degrees of freedom must be explicitly included in the theoretical description of the collision. In spite of this, permanent shape deformations, collective surface vibrational modes, and nucleon (multi-nucleon) transfer channels have proven to be most relevant

✉ Manjeet Singh Gautam
gautammanjeet@gmail.com

[1] Department of Physics, Indus Degree College, Kinana, Jind, Haryana 126102, India

[2] Department of Physics, Dr. B. R. Ambedekar Institute of Technology, Port Blair, Andaman & Nicobar 744103, India

channels, which in turn, modify quantum tunneling and consequently lead to larger fusion cross sections by several orders of magnitude over the predictions of the single barrier penetration model [12–15]. In the eigen-channel approach, the coupling to such intrinsic channels results in the replacement of nominal fusion barrier by a distribution of the potential barriers of different height and weight; henceforth, the channel coupling effects can be beautifully correlated with the observed fusion enhancement of various heavy ion fusion reactions around the Coulomb barrier [16–18].

In a fusion process, the most difficult problem is to include all channels simultaneously in the theoretical description. However, it is very interesting to account for the effects of the relevant channels only. The influences of static deformations and/or inelastic surface vibrations in the enhancement of sub-barrier fusion cross section have been well accounted by the theoretical models [6, 16–18]. For instance, the authors of refs. [19–21] clearly identified the role of low lying inelastic surface excitations in the fusion process, whereas the impacts of static and dynamical deformations are directly evident from the fusion dynamics involving *Sm*-target isotopes [4, 6, 13, 14, 17, 22–27]. With the increase of the target isotopic mass, there is a structural change of the *Sm* isotopes from spherical to a statically deformed shapes. For the lightest targets $\left({}^{144,148}_{62}Sm\right)$, the collective surface vibrational modes are found to dominate the couplings, while in heaviest targets $\left({}^{150,152,154}_{62}Sm\right)$, the rotational states, rather than vibrational excitations, are responsible for the isotopic enhancement of sub-barrier fusion [4, 6, 13, 14, 17, 22–27]. Thus, the fusion of *Sm* isotopes with different projectiles represents an ideal opportunity for testing theoretical models. Keeping this view, this work analyzes the fusion of the ${}^{16}_{8}O + {}^{144,148,150,152,154}_{62}Sm$ systems, using the coupled channel approach [28] and the energy-dependent Woods-Saxon potential model (EDWSP) model [3, 7, 20, 29, 30].

It is well known that the abovementioned fusing systems are stable against breakup effects. Therefore, it is quite interesting to study the fusion of loosely bound projectiles with the *Sm* isotopes. Recently, Rath et al. [31–33] have measured the complete fusion excitation function in ${}^{6,7}_{3}Li + {}^{144,152}_{62}Sm$ reactions. They found that the complete fusion data at above - barrier energies is suppressed due to projectile breakup effects. The authors use the recoil catcher technique followed by off-line gamma-ray spectrometer to perform precise measurements of the fusion cross section and claimed that the inhibition of complete fusion of the ${}^{6}_{3}Li + {}^{152}_{62}Sm\left({}^{7}_{3}Li + {}^{152}_{62}Sm\right)$ system at above-barrier energies is of 28% (25%). The projectiles $\left({}^{6,7}_{3}Li\right)$ are weakly bound due to their low threshold of the *alpha*-breakup channel and consequently the amount of the incident flux going into the complete fusion channel is reduced [33, 34]. The missing complete fusion cross sections appears as incomplete fusion. Several conflicting experimental and theoretical findings about the enhancement and the suppression of fusion in collisions of loosely bound nuclei have been reported in the literature [35–39]. For instance, the authors of refs. [40–43] predicted the enhancement of the fusion cross sections due to breakup effects, while in other studies, the authors suggested an inhibition of the complete fusion data at above - barrier energies when compared with the theoretical expectations [44–48]. Such suppression effects can be correlated with the breakup of the projectile before reaching the fusion barrier, with either one or both breakup fragment being captured by the target, leading to partial or complete fusion yields [44–48]. In this regard, we have analyzed the fusion dynamics of ${}^{6,7}_{3}Li + {}^{152}_{62}Sm$ reactions, where the fusion suppression factor of the order of 28% (25%) for the ${}^{6}_{3}Li + {}^{152}_{62}Sm\left({}^{7}_{3}Li + {}^{152}_{62}Sm\right)$ collision at above - barrier energies has been found in the literature. In this work, the calculations are done by the EDWSP model and the coupled channel model. Interestingly, the EDWSP model based calculations estimate the suppression factor to be 15% (17%) for ${}^{6}_{3}Li + {}^{152}_{62}Sm$ $\left({}^{7}_{3}Li + {}^{152}_{62}Sm\right)$ system, which is smaller than the reported values. In contrast, the sub-barrier fusion enhancement of the studied reactions occurs as a consequence of the channel coupling effects and hence reasonably recovered by the adopted model calculations. The brief description of the method of calculation is given in Sect. 2. The results are discussed in detail in Sect. 3 while the conclusions drawn are discussed in Sect. 4.

## 2 Theoretical Formalism

The total fusion cross section can be estimated by using the following expression

$$\sigma_{\mathrm{F}} = \frac{\pi}{k^2}\sum_{\ell=0}^{\infty}(2\ell+1)T_{\ell}^{F} \tag{1}$$

Based on parabolic approximation, Hill and Wheeler [49] proposed an expression for tunneling probability $\left(T_{\ell}^{F}\right)$ and is defined as

$$T_{\ell}{}^{F} = \frac{1}{1+\exp\left[\frac{2\pi}{\hbar\omega_{\ell}}(V_{\ell}-E)\right]} \tag{2}$$

This parabolic approximation was further simplified by Wong using certain assumptions for barrier position, barrier height, and barrier curvature and obtains the following formula for evaluation of fusion excitation functions [50]

$$\sigma_{\mathrm{F}} = \frac{\hbar\omega R_{\mathrm{B}}^{2}}{2E}\ell n\left[1+\exp\left(\frac{2\pi}{\hbar\omega}(E-V_{\mathrm{B}})\right)\right] \tag{3}$$

In the recent works, it has been well recognized that the EDWSP model is an efficient theoretical tool to explore the sub-barrier fusion dynamics [3, 7, 20, 29, 30, 51]. This work makes the use of the standard Woods-Saxon potential to analyze the available fusion data. The standard Woods-Saxon potential is described via three parameters and is defined as

$$V_{\mathrm{N}}(r) = \frac{-V_0}{\left[1+\exp\left(\frac{r-R_0}{a}\right)\right]} \tag{4}$$

with $R_0 = r_0\left(A_{\mathrm{P}}^{\frac{1}{3}} + A_{\mathrm{T}}^{\frac{1}{3}}\right)$ as radius parameter. $V_0$ is strength and $a$ is diffuseness of the Woods-Saxon potential. In the EDWSP model, $V_0$ is defined as

$$V_o = \left[A_{\mathrm{P}}^{\frac{2}{3}} + A_{\mathrm{T}}^{\frac{2}{3}} - (A_{\mathrm{P}} + A_{\mathrm{T}})^{\frac{2}{3}}\right]\left[2.38 + 6.8(1 + I_{\mathrm{P}} + I_{\mathrm{T}})\frac{A_{\mathrm{P}}^{\frac{1}{3}}A_{\mathrm{T}}^{\frac{1}{3}}}{\left(A_{\mathrm{P}}^{\frac{1}{3}} + A_{\mathrm{T}}^{\frac{1}{3}}\right)}\right] \mathrm{MeV} \tag{5}$$

where $I_{\mathrm{P}} = \left(\frac{N_{\mathrm{P}}-Z_{\mathrm{P}}}{A_{\mathrm{P}}}\right)$ and $I_{\mathrm{T}} = \left(\frac{N_{\mathrm{T}}-Z_{\mathrm{T}}}{A_{\mathrm{T}}}\right)$ are the isospin asymmetry of the colliding systems.

In the EDWSP model, the energy-dependent diffuseness parameter is defined as

$$a(E) = 0.85\left[1 + \frac{r_0}{13.75\left(A_{\mathrm{P}}^{-\frac{1}{3}} + A_{\mathrm{T}}^{-\frac{1}{3}}\right)\left(1+\exp\left(\frac{\frac{E}{V_{\mathrm{B}0}}-0.96}{0.03}\right)\right)}\right] \mathrm{fm} \tag{6}$$

The range parameter ($r_0$) is strongly affected by the nature of dominant channel coupling effects. Three potential parameters ($r_0$,$a$, and $V_0$) are intrinsically interrelated, and the variation in one automatically brings the corresponding adjustments in the values of the other parameters [3, 7, 20, 29, 30]. In the present model, the depth ($V_0$) can be obtained by using the Eq. (5) while other two parameters are mathematically related with each other via Eq. (6). The range of diffuseness parameter is controlled by the range parameter ($r_0$) which geometrically defines the radii of the fusing systems through $R_0 = r_0\left(A_{\mathrm{P}}^{\frac{1}{3}} + A_{\mathrm{T}}^{\frac{1}{3}}\right)$. Furthermore, the fluctuations in the diffuseness are directly linked with the variations of radii of the colliding systems during their nuclear interactions. It is relevant to mentioned here that the values of range parameter used in the EDWSP model calculations are consistent with the commonly adopted values ranging from $r_0 = 0.90$ fm to $r_0 = 1.35$ fm [16, 17, 52–58].

Theoretically, the influences of channel coupling effects on fusion process can only be judged by using the theoretical models based on the coupled channel methods. In the coupled channel approach, the non-elastic channels associated with the colliding pairs are coupled with their relative motion and one can estimate the impacts of nuclear structure effects on fusion process. Although, it is very difficult to include the effects of all intrinsic channels, it is fruitful to entertain the relevant intrinsic channels in the theoretical calculations [28, 59, 60]. In this work, the coupled channel calculations have been performed by opting the code CCFULL [28] wherein the coupled channel equations are solved numerically by adopting rotating frame approximation and ingoing wave boundary conditions (IWBC) [28, 59, 60]. The following set of coupled channel equations are to be solved in the coupled channel approach.

$$\left[\frac{-\hbar^2}{2\mu}\frac{d^2}{dr^2} + \frac{J(J+1)\hbar^2}{2\mu r^2} + V_{\mathrm{N}}(r) + \frac{Z_{\mathrm{P}}Z_{\mathrm{T}}e^2}{r} + \varepsilon_{\mathrm{n}} - E_{\mathrm{cm}}\right]\psi_{\mathrm{n}}(r) + \sum_{\mathrm{m}} V_{\mathrm{nm}}(r)\,\psi_{\mathrm{m}}(r) = 0 \tag{7}$$

where, $\overrightarrow{r}$ is the radial coordinate for the relative motion between fusing nuclei. $\mu$ is defined as the reduced mass of the projectile-target system. $E_{\mathrm{cm}}$ and $\varepsilon_{\mathrm{n}}$ represent the bombarding energy in the center of mass frame and the excitation energy of the $n$th channel respectively. The $V_{\mathrm{n\,m}}$ is the matrix elements of the coupling Hamiltonian, which in the collective model consists of the Coulomb and nuclear components. By employing the rotating frame approximation and the IWBC, one can obtain the numerical solution of the coupled channel equations. The code CCFULL makes the use of static Woods-Saxon potential for the calculations of fusion cross sections; and therefore, by taking in account of all the relevant channels, the fusion cross section can be written as

$$\sigma_{\mathrm{F}}(E) = \sum_J \sigma_J(E) = \frac{\pi}{k_0^2}\sum_J (2J+1)P_J(E) \tag{8}$$

where, $P_J(E)$ is the total transmission coefficient corresponding to the angular momentum $J$.

## 3 Results and Discussion

The significance of barrier modification effects that originate due to energy dependence in the nucleus-nucleus potential and nuclear structure effects in the fusion dynamics of ${}^{16}_{8}O + {}^{144,148,150,152,154}_{62}Sm$ and ${}^{6,7}_{3}Li + {}^{152}_{62}Sm$ reactions is highlighted by opting the coupled channel model and the EDWSP method. The values of the deformation parameters and corresponding excitation energies for low lying $2^+$ and $3^-$ vibrational states of the chosen nuclei are listed in Table 1. The rotational states of the deformed target nuclei along with their corresponding rotational energies and higher deformation such as hexadecapole deformation are listed in Table 2. In Table 3, the values of range, depth, and diffuseness of the EDWSP model calculations for various fusing systems are listed. The barrier

**Table 1** The deformation parameter ($\beta_\lambda$) and the energy ($E_\lambda$) of the quadrupole and octupole vibrational states of various nuclei

| Nucleus | $\beta_2$ | $E_2$ (MeV) | $\beta_3$ | $E_3$ (MeV) | Reference |
|---|---|---|---|---|---|
| $^{144}_{62}Sm$ | 0.110 | 1.660 | 0.210 | 1.810 | [6] |
| $^{148}_{62}Sm$ | 0.140 | 0.555 | 0.190 | 1.160 | [6] |
| $^{150}_{62}Sm$ | 0.190 | 0.333 | 0.110 | 1.071 | [22] |

height, barrier position, and barrier curvature of the fusing nuclei, which are obtained from the uncoupled potential used in the CCFULL calculations in no coupling limit, are listed in Table 4. These parameters are used in the EDWSP model calculations along with the Wong formalism.

The modifications of barrier characteristics such as barrier height, barrier position, and barrier curvature for $^{16}_{8}O + ^{144,154}_{62}Sm$ reactions are shown in Fig. 1a–d. The similar results are found for other projectile-target combinations, and hence are not shown. The longer tail of the fusion barrier for $^{16}_{8}O + ^{154}_{62}Sm$ reaction (Fig. 1c) in comparison to that of $^{16}_{8}O + ^{144}_{62}Sm$ reaction (Fig. 1a) indicates that fusion process starts at larger internuclear separation for former system than that of the later system. Such results are also consistent from the nuclear structure of $^{144,148,150,152,154}_{62}Sm$ isotopes, wherein the lighter target has spherical symmetry $\left(^{144}_{62}Sm\right)$, while the heavier targets are statically deformed in shape $\left(^{150,152,154}_{62}Sm\right)$. Among the chosen isotopes, the degree of static deformation is largest for $^{144}_{62}Sm$ nucleus and consequently has larger spatial extension along a particular direction. In EDWSP calculations, as listed in Table 3, the magnitude of the range parameter ($r_0$) is of increasing order as one move from $^{16}_{8}O + ^{144}_{62}Sm$ reaction to $^{16}_{8}O + ^{154}_{62}Sm$ reaction, which in turn, predicts substantially large fusion enhancement at below barrier energies for $^{16}_{8}O + ^{154}_{62}Sm$ reaction in comparison to that of $^{16}_{8}O + ^{144}_{62}Sm$ reaction. At below barrier energies, the largest diffuseness ($a = 0.97$ fm) for $^{16}_{8}O + ^{154}_{62}Sm$ reaction ($a = 0.95$ fm for $^{16}_{8}O + ^{144}_{62}Sm$ reaction) produces lowest fusion barrier, henceforth, allows the shifting of maximum flux from incoming channel to fusion channel. For instance, the lowest fusion barrier

**Table 2** The deformation parameter ($\beta_\lambda$) and the energy ($E_\lambda$) of the static deformation of the deformed nuclei

| Nucleus | $\beta_2$ | $E_2$ (MeV) | $\beta_4$ | Reference |
|---|---|---|---|---|
| $^{150}_{62}Sm$ | 0.250 | 0.334 | 0.050 | [24] |
| $^{152}_{62}Sm$ | 0.280 | 0.112 | 0.050 | [24] |
| $^{154}_{62}Sm$ | 0.330 | 0.082 | 0.050 | [24] |

**Table 3** Range, depth, and diffuseness of Woods-Saxon potential used in the present calculations for various systems [29, 30]

| System | $r_0$ (fm) | $V_0$ (M e V) | $\frac{a^{present}}{energy \quad range}\left(\frac{a^{present}}{energy \quad range}\right)$ |
|---|---|---|---|
| $^{16}_{8}O + ^{144}_{62}Sm$ | 1.110 | 67.68 | $\frac{0.95\text{ to }0.85}{55\text{ to }95}$ |
| $^{16}_{8}O + ^{148}_{62}Sm$ | 1.120 | 69.30 | $\frac{0.95\text{ to }0.85}{53\text{ to }77}$ |
| $^{16}_{8}O + ^{150}_{62}Sm$ | 1.135 | 70.09 | $\frac{0.96\text{ to }0.85}{52\text{ to }75}$ |
| $^{16}_{8}O + ^{152}_{62}Sm$ | 1.140 | 70.86 | $\frac{0.96\text{ to }0.85}{52\text{ to }70}$ |
| $^{16}_{8}O + ^{154}_{62}Sm$ | 1.145 | 71.62 | $\frac{0.97\text{ to }0.85}{50\text{ to }101}$ |
| $^{6}_{3}Li + ^{152}_{62}Sm$ | 1.075 | 34.00 | $\frac{0.94\text{ to }0.85}{18\text{ to }40}$ |
| $^{7}_{3}Li + ^{152}_{62}Sm$ | 1.075 | 42.11 | $\frac{0.94\text{ to }0.85}{18\text{ to }40}$ |

produced for $^{16}_{8}O + ^{154}_{62}Sm$ reaction is 57.42 MeV $\left(\text{FB} = 59.70\text{ MeV for } ^{16}_{8}O + ^{144}_{62}Sm\right)$ as depicted in Fig. 1. Further, with the increase of the bombarding energy, the diffuseness parameter gradually decreases and this decrease is compensated by increasing the height of the corresponding fusion barrier, and thus, variations in both are saturated in above barrier energy regions. At well above barrier energies, the variations in diffuseness and corresponding fusion barrier cease which ultimately leads to overlapping of the predictions due to different theoretical methods. This reflects the insensitivity of the fusion data toward channel coupling effects. The authors of refs. [56, 57] based on density-constrained time-dependent Hartree-Fock theory (DC-TDHF) have shown that the channel coupling effects and the coordinate-dependent mass modify the phenomenological ion-ion potential and generate the energy dependence in nucleus-nucleus potential. In this approach, the spectrum of the energy-

**Table 4** Fusion barrier parameters like $V_{B0}$, $R_{B,}$ and $\hbar\omega$ obtained from the uncoupled potential used in the CCFULL calculations for various heavy ion systems

| System | $V_{B0}$ (MeV) | $R_B$ (fm) | $\hbar\omega$ (MeV) | Reference |
|---|---|---|---|---|
| $^{16}_{8}O + ^{144}_{62}Sm$ | 61.11 | 10.23 | 4.23 | [28] |
| $^{16}_{8}O + ^{148}_{62}Sm$ | 59.59 | 11.26 | 4.45 | [28] |
| $^{16}_{8}O + ^{150}_{62}Sm$ | 59.62 | 11.26 | 4.48 | [28] |
| $^{16}_{8}O + ^{152}_{62}Sm$ | 59.46 | 11.30 | 4.47 | [28] |
| $^{16}_{8}O + ^{154}_{62}Sm$ | 59.41 | 10.81 | 4.50 | [28] |
| $^{6}_{3}Li + ^{152}_{62}Sm$ | 25.10 | 9.98 | 5.05 | [28] |
| $^{7}_{3}Li + ^{152}_{62}Sm$ | 24.40 | 10.32 | 4.61 | [28] |

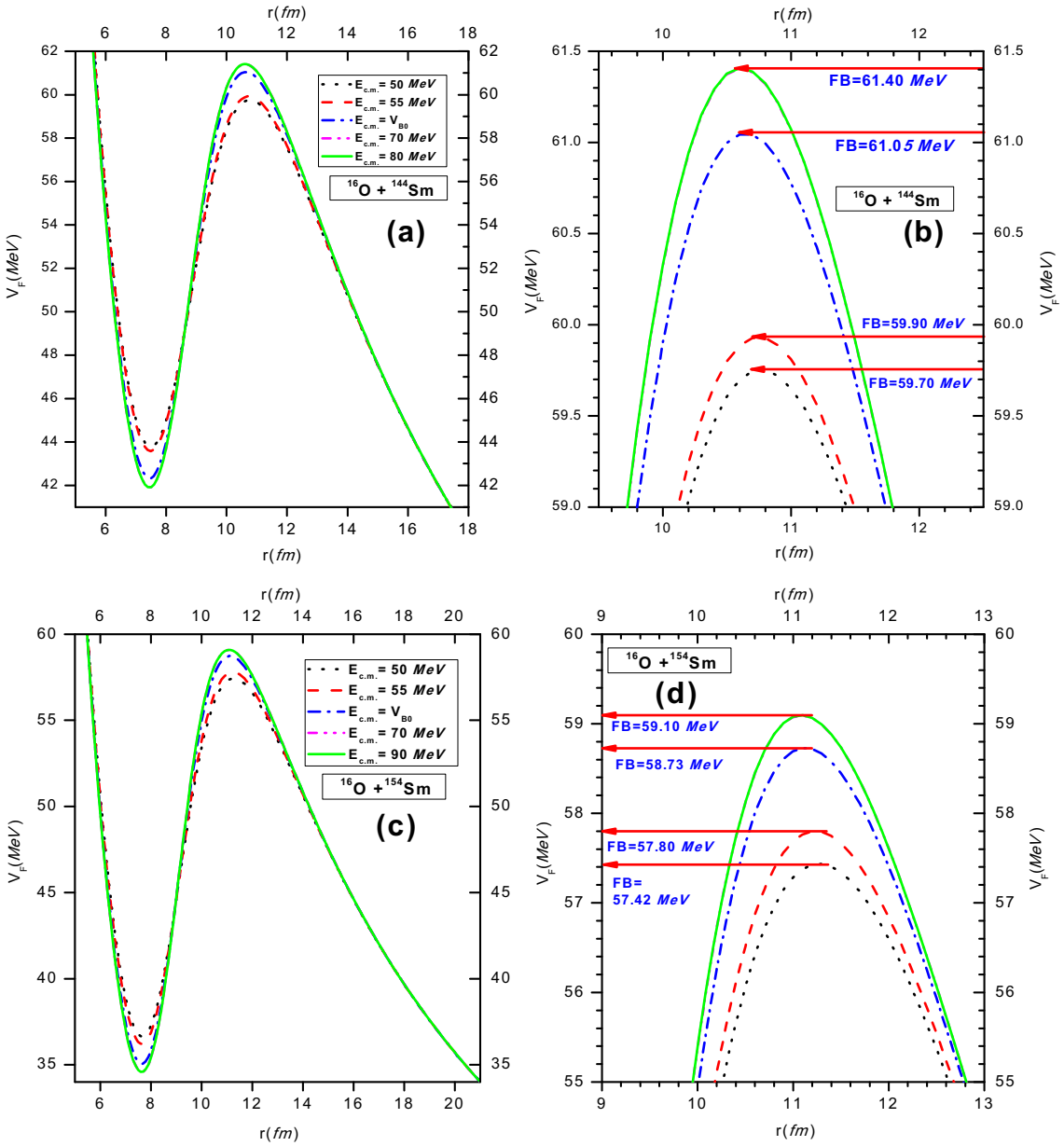


**Fig. 1** The fusion barrier (FB) for ${}^{16}_{8}O + {}^{144}_{62}Sm$ (**a**, **b**) and ${}^{16}_{8}O + {}^{154}_{62}Sm$ systems (**c**, **d**) obtained using the EDWSP model [29, 30]. The similar results are found for the ${}^{16}_{8}O + {}^{148,150,154}_{62}Sm$ reactions

dependent fusion barriers is produced and as a consequence of dynamically lowering of the effective fusion barrier, DC-TDHF approach adequately explained the fusion dynamics of various heavy ion fusion reactions. In similar way, in the essence of the production of spectrum of energy-dependent fusion barrier of variable height, the EDWSP model reasonably explored the observed fusion dynamics of the chosen reactions.

As far as projectile $\left({}^{16}_{8}O\right)$ is concerned, it is doubly magic and possesses low lying inelastic surface excitations as most relevant intrinsic channels. But due to high excitation energy, their influences on fusion process are expected to be very weak and thus the effects of the target degrees of freedom are directly inferred from the fusion dynamics of ${}^{16}_{8}O + {}^{144,148,150,152,154}_{62}Sm$ reactions. In case of ${}^{16}_{8}O + {}^{144,148}_{62}Sm$ reactions, the colliding nuclei are spherical in shape and the coupling to low lying collective excitations like $2^+$ and $3^-$ vibrational states play a crucial role in the enhancement of the fusion excitation functions at below barrier energies over the expectations of the one-dimensional barrier penetration model. The experimentally observed data is substantially larger than the no coupling calculations obtained by treating the colliding pairs as inert systems. The coupling to one phonon $2^+$ vibrational state improves the calculated results but unable to bring the close agreement with the below barrier fusion

data, while the above barrier fusion data has been reasonably recovered by such calculations as evident from Fig. 2. For addressing the sub-barrier fusion data, the inclusions of more intrinsic channels are necessarily required. The addition of the one phonon $2^+$ and $3^-$ vibrational states along with their mutual couplings such as $(2^+ \times 3^-)$ reproduces the fusion enhancement of ${}^{16}_{8}O + {}^{144,148}_{62}Sm$ systems [6, 13, 14, 17, 22–25]. In ${}^{144,148}_{62}Sm$ isotopes, the impacts of the anharmonicities associated with the low lying inelastic surface excitations on fusion process have been pointed out in literature [61–64]. For ${}^{144}_{62}Sm$ isotope, the presence of anharmonicities in the low lying quartet states, which seems to correspond to the double octupole phonon excitations, strongly modifies the energy dependence of tunneling probability as well as the fusion cross section. The authors [61, 62] explicitly showed that the addition of the double-phonon coupling spoils agreement between the data and theory. Thus, in case of ${}^{16}_{8}O + {}^{144}_{62}Sm$ system, the fusion cross sections data is quite sensitive to the presence of considerably large anharmonicities in the octupole surface vibrations of the target isotope and must be entertained in the numerical calculations in order to achieve good description of the fusion data. For ${}^{16}_{8}O + {}^{148}_{62}Sm$ system [61–64], the target nucleus $\left({}^{148}_{62}Sm\right)$ also exhibits anharmonic surface vibrations and possesses negative and positive static quadrupole moments for the first $2^+$ and $3^-$ vibrational states respectively. Therefore, the coupling to such vibrational states produces larger sub-barrier fusion enhancement of ${}^{16}_{8}O + {}^{148}_{62}Sm$ system. On the other hand, the EDWSP model calculations reasonably address the fusion data of ${}^{16}_{8}O + {}^{144,148}_{62}Sm$ systems in the domain of the Coulomb barrier, which in turn automatically accommodate the effects of the anharmonicities associated with the collective states as well as the influences of the low lying inelastic surface excitations of the target isotopes as depicted in Fig. 2.

For ${}^{16}_{8}O + {}^{150}_{62}Sm$ system, the coupled channel calculations are performed by treating the spherical as well as statically deformed choice of the target isotope. The no coupling calculations, wherein the collision partners are taken as an inert, are much smaller than the fusion data particularly at below barrier energies. The inclusion of the one phonon $2^+$ and $3^-$ vibrational states along with their mutual coupling is unable to describe the observed fusion dynamics. This clearly indicates that the higher order vibrational states, like two phonon, three-phonon states are required to achieve good agreement between theoretical calculations and experimental data. However, the addition of two-phonon and three-phonon states in target does not bring additional sub-barrier fusion enhancement. The ${}^{150}_{62}Sm$ isotope lies in the region of the structural change of *Sm* isotopes from spherical symmetry to a statically deformed shape. Therefore, it is reasonable to test the effects of rotational states of the target isotope on fusion process. Interestingly, the coupling to rotational states up to $10^+$ ground state rotational band having $\beta_2 = 0.250$ and $\beta_4 = 0.005$ for ${}^{150}_{62}Sm$ nucleus reproduces the fusion enhancement of ${}^{16}_{8}O + {}^{150}_{62}Sm$ system and hence unambiguously indicates the dominance of rotational states associated with target isotope over its vibrational states as evident from Fig. 3.

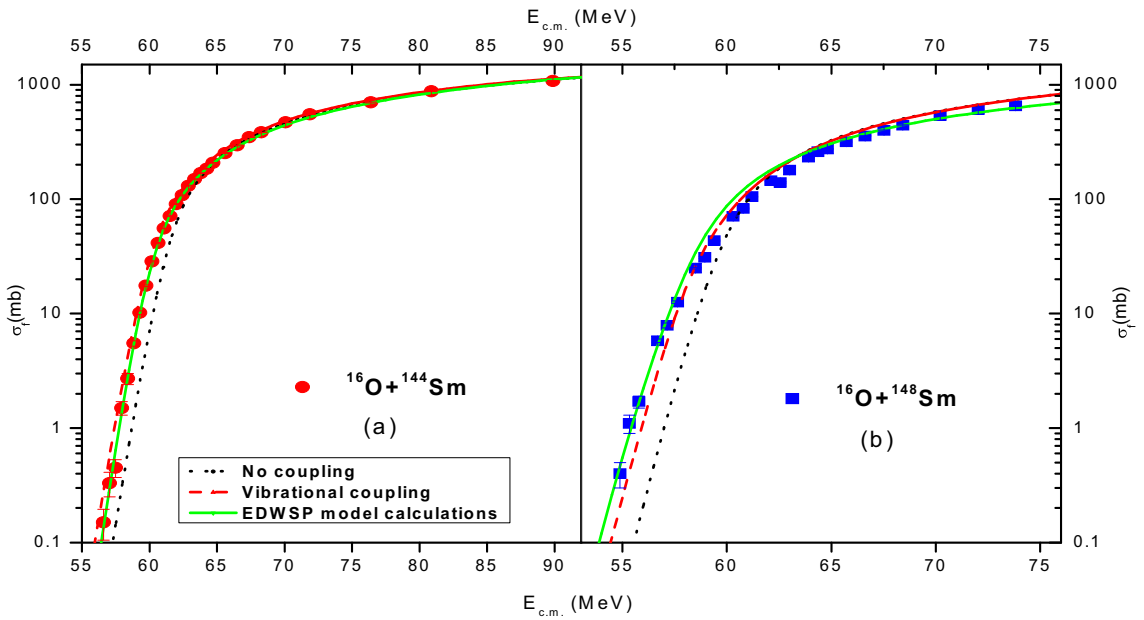


**Fig. 2** The fusion excitation functions of ${}^{16}_{8}O + {}^{144}_{62}Sm$ (**a**) and ${}^{16}_{8}O + {}^{148}_{62}Sm$ (**b**) reactions obtained using the EDWSP model [29, 30] and the coupled channel code CCFULL [28]. The results are compared with available experimental data taken from ref. [6]

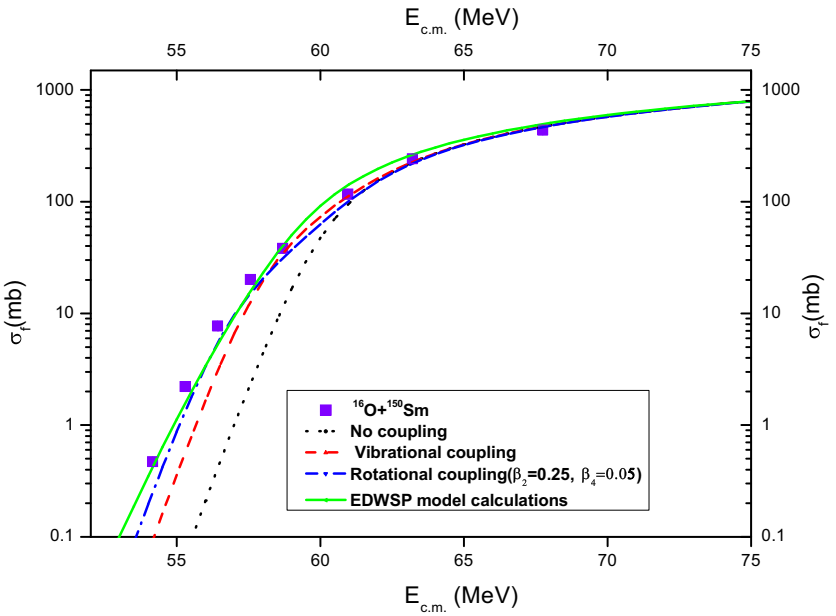


**Fig. 3** The fusion excitation functions of ${}^{16}_{8}O + {}^{150}_{62}Sm$ reaction obtained using the EDWSP model [29, 30] and the coupled channel code CCFULL [28]. The results are compared with available experimental data taken from ref. [60]

In fusion of ${}^{16}_{8}O + {}^{152,154}_{62}Sm$ systems, the targets $\left({}^{152,154}_{62}Sm\right)$ are statically deformed, wherein the rotational states of targets are playing a crucial role in fusion process. The coupling to such relevant channels produces substantially large fusion enhancement over the expectations of the single barrier penetration model. In case of ${}^{16}_{8}O + {}^{152,154}_{62}Sm$ reactions, the no coupling calculations predict very small sub-barrier fusion cross section in comparison to the experimental data, while the above barrier fusion data can be reasonably recovered within the view of no coupling calculations. In theoretical analysis of deformed nuclei, the vibrational model is not suited. The couplings to rotational states (up to $10^+$ ground state rotational bands of the target isotopes) lead to significantly larger fusion cross sections with reference to the no coupling calculations, but still there remain large discrepancies between the coupled channel treatment and the below barrier fusion data. The inclusions of rotational states higher than $10^+$ ground state rotational bands are unable to produce the additional fusion enhancement, and hence more intrinsic channels such as higher order deformations are required in order to achieve the close agreement with the experimental data. In literature, it has been well populated that the heavier targets $\left({}^{152,154}_{62}Sm\right)$ exhibit higher order deformation such as $\beta_2$,$\beta_4$, and $\beta_6$ deformation but the effects of $\beta_6$ deformation are quite small in comparison to that of $\beta_4$-deformation. Therefore, the larger fraction of the sub-barrier fusion enhancement of ${}^{16}_{8}O + {}^{152,154}_{62}Sm$ reactions can be attributed to the coupling to rotational states and hexadecapole deformation of the target isotopes.

In present treatment, we include the impact of rotational states in ground state rotational band as well as $\beta_4$-deformation associated with the target isotope. In ${}^{16}_{8}O + {}^{152,154}_{62}Sm$ reactions, the coupling to rotational states up to $10^+$ ground state rotational band having $\beta_2 = 0.280$ and $\beta_4 = 0.005$ for ${}^{152}_{62}Sm$ nucleus, while $\beta_2 = 0.330$ and $\beta_4 = 0.005$ for ${}^{154}_{62}Sm$ nucleus result in reasonable addressal of the fusion data in the whole range of energy spread across the Coulomb barrier [Fig. 4]. The small discrepancies between the coupled channel calculations and the experimental data in deep sub-barrier energy regions can be correlated with the existence of the non-zero values of $\beta_6$-deformation which must be incorporated in order to achieve the good description of the fusion dynamics [17]. In contrast, in the EDWSP model calculations, the barrier modification effects, which are induced due to the energy dependence in nucleus-nucleus potential, account for the fusion enhancement of ${}^{16}_{8}O + {}^{150,152,154}_{62}Sm$ reactions. The larger sub-barrier fusion enhancement of ${}^{16}_{8}O + {}^{150,152,154}_{62}Sm$ systems in comparison to that of ${}^{16}_{8}O + {}^{144,148}_{62}Sm$ systems can be ascribed to the dominance of static deformation over the collective excitations of the target isotopes [6, 13, 14, 17, 22–27, 65]. In the $O + Sm$ reactions, the colliding pairs are stable against breakup effects; henceforth, the above barrier complete fusion data of $O + Sm$ reactions is not suppressed with respect to the theoretical expectations. Therefore, within the view of present model calculations, it is quite interesting to analyze the fusion dynamics of ${}^{6,7}_{3}Li + {}^{152}_{62}Sm$ reactions, wherein the projectiles display breakup effects on the fusion process. The barrier modification effects introduced here [Fig. 5] have close resemblance to that of $O + Sm$ reactions as already discussed in Fig. 1.

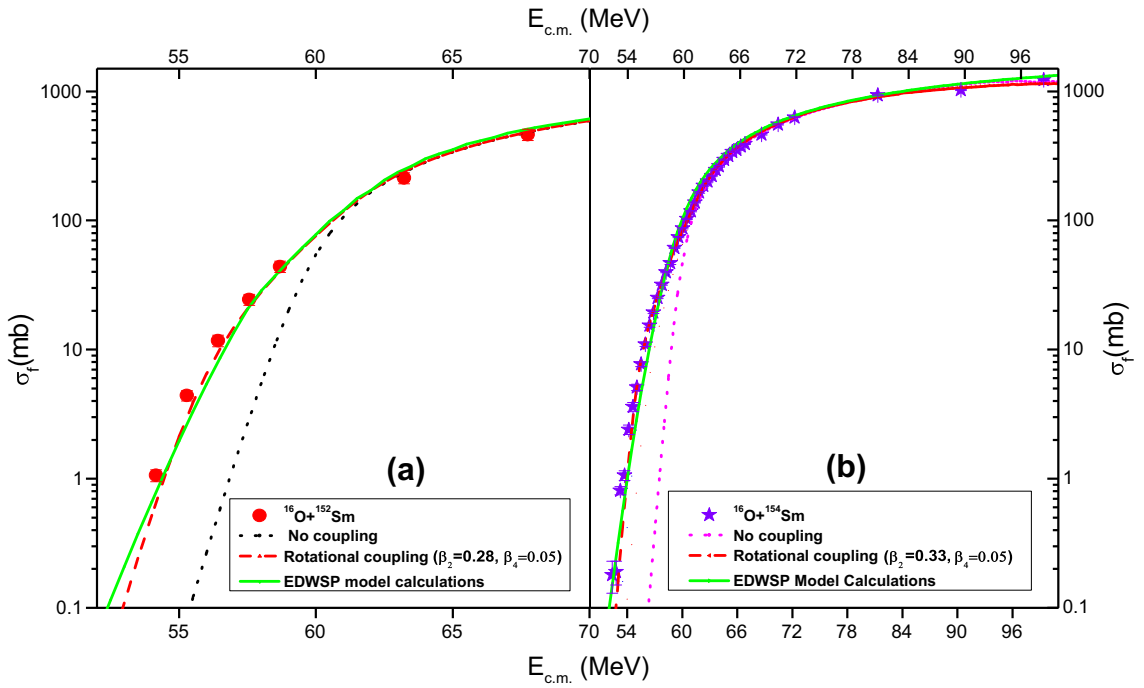


**Fig. 4** The fusion excitation functions of ${}^{16}_{8}O + {}^{152}_{62}Sm$ (**a**) and ${}^{16}_{8}O + {}^{154}_{62}Sm$ (**b**) reactions obtained using the EDWSP model [29, 30] and the coupled channel code CCFULL [28]. The results are compared with available experimental data taken from refs. [6, 60]

The coupled channel calculations for ${}^{6,7}_{3}Li + {}^{152}_{62}Sm$ reaction are shown in Fig. 6. As far as the projectiles $\left({}^{6,7}_{3}Li\right)$ are concerned, they are loosely bound nuclei and display the signature of the breakup effects, while the target isotope $\left({}^{152}_{62}Sm\right)$ rules out such possibilities due to stability against breakup effects. In case of ${}^{6}_{3}Li + {}^{152}_{62}Sm$ system, no coupling calculations are significantly smaller than the experimental data. By taking projectile as inert, the inclusion of rotational states up to $10^+$ ground state rotational band improves the results but still there are large discrepancies between theory and fusion data at below barrier energies. Rath et al. [32] have explicitly shown that the higher order deformation such as $\beta_2$ and $\beta_4$-deformation associated with the ${}^{152}_{62}Sm$ isotope is playing an important role in the fusion dynamics of the given reaction. The inclusion of rotational states up to $10^+$ ground state rotational band having $\beta_2 = 0.280$ and $\beta_4 = 0.005$ for the ${}^{152}_{62}Sm$ nucleus significantly enhances the magnitude of fusion cross sections and brings theoretical calculations nearer to the fusion data. However, the additions of more intrinsic channels are needed

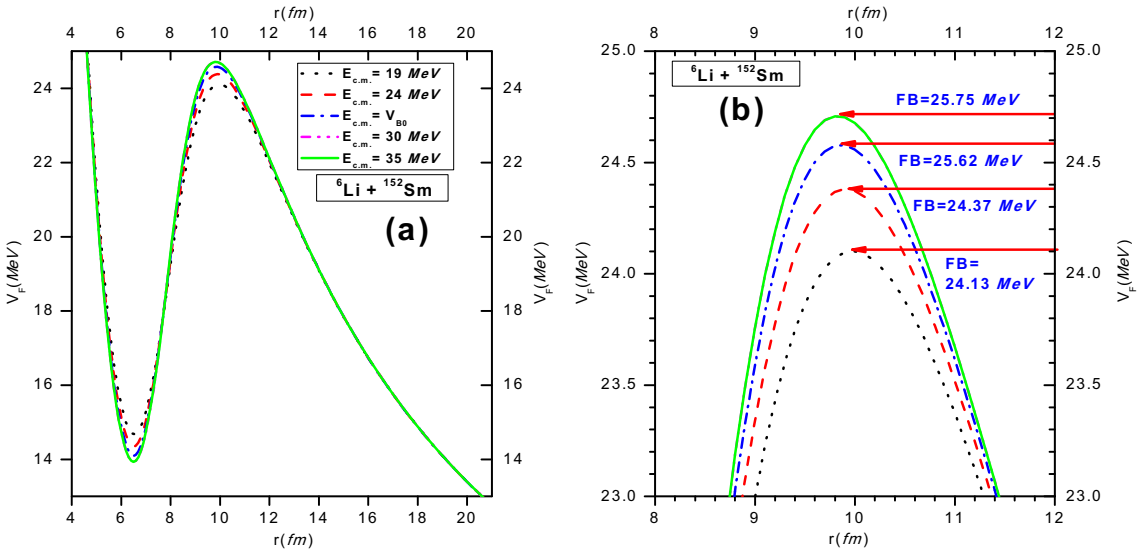


**Fig. 5** (a) The fusion barrier (FB) for ${}^{6}_{3}Li + {}^{152}_{62}Sm$ system (b) obtained using the EDWSP model [29, 30]

to account for the explanation of the observed fusion enhancement. To address the below barrier fusion data, the projectile excitations must be incorporated. The projectile exhibits a non-zero quadrupole moment ($Q_m = -0.082\,fm^2$) in its ground state and also the unbound first excited state ($3^+$, 2.186 MeV). The spectroscopic analysis suggested a non-zero transition probability ($BE\,2, 1^+ \rightarrow 3^+$) of the order of $21.80\,e^2$ fm$^4$ for $3^+$ excited states of the projectile which lies at the excitation energy of $2.186 MeV$ [31–34, 48]. Therefore, the inclusion of $3^+$ excited state of the projectile along with rotational states as well as higher deformation of the target recovers fusion data in a reasonable way. This shows that the below barrier complete fusion data can only be addressed if one includes the collective vibrational modes and/or static deformations of the colliding pairs. However, at the cost of good addressal of the experimental data, the complete fusion data at above barrier energies for ${}^{6}_{3}Li + {}^{152}_{62}Sm$ system gets suppressed with respect to the coupled channel calculations. The authors [48] with continuum discretized coupled channel (CDCC) approach [66–68] have pointed out the breakup of the projectile in the entrance channel and consequently explained the fusion dynamics of ${}^{6}_{3}Li + {}^{90}_{40}Zr$ reaction by treating projectile $\left({}^{6}_{3}Li\right)$ as two body $a + d$ cluster structure with a breakup threshold of $1.475 MeV$. The breakup of the projectile into $a + d$ cluster structure is also supported by the experimental investigations of Signorini et al. [69]. Otomar et al. [70, 71] performed the CDCC calculations for ${}^{6}_{3}Li + {}^{144}_{62}Sm$ reaction and confirms the $a + d$ cluster structure model for the projectile. The breakup channel results in the production of repulsive polarization potential and consequently increases the barrier height and reduces the complete fusion yields. Furthermore, authors pointed out that at low energies, the breakup process occurs due to the dominance of the Coulomb force for all scattering angles. As incident energy reaches to above barrier energies, the contribution from the Coulomb breakup decreases, while nuclear breakup becomes dominant at larger angles [70, 71]. The recent experimental measurements have been shown that the transfer process followed by breakup of the projectile may predominate over the breakup of stable weakly bound system at below barrier energies [72–74]. To estimate the breakup fraction in complete fusion for ${}^{6}_{3}Li$ -induced reactions, Elmahdy et al. [75] analyzed the coupled channel calculations for complete fusion yields using the distorted wave Born approximation (DWBA). On theoretical ground, the authors have shown that the enhancement of breakup cross section at above barrier energies increases with the increase of charge and mass numbers. Due to long ranged Coulomb force, the Coulomb breakup dominates at below barrier energies while the nuclear breakup contributes up to grazing collisions. For weakly bound systems, breakup itself cannot result enough suppression of fusion cross section at near and sub-barrier energies, and therefore, it is necessary to take into account of the transfer channels which are well populated at above barrier energies. It is quite interesting to note that in case of weakly bound nuclei, the dynamic polarization potential produced due to breakup effects is of repulsive nature in the nuclear surface region for all incident energies, and hence, authors claimed that the above barrier complete fusion data is inhibited with respect to the theoretical predictions by 28% [32] as evident from Fig. 6a.

In case of ${}^{7}_{3}Li + {}^{152}_{62}Sm$ reaction, the same rotational degrees of freedom as used for ${}^{6}_{3}Li + {}^{152}_{62}Sm$ system have been

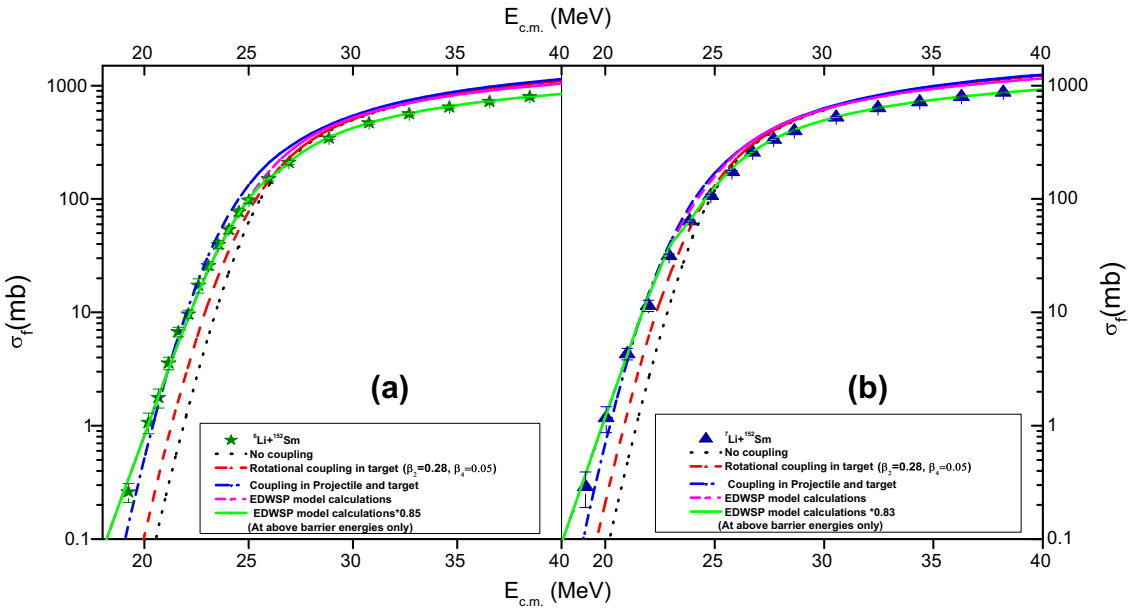


**Fig. 6** (a) The fusion excitation functions of ${}^{6,7}_{3}Li + {}^{152}_{62}Sm$ reactions (b) obtained using the EDWSP model [29, 30] and the coupled channel code CCFULL [28]. The results are compared with the available experimental data taken from refs. [32, 33]

adopted for target nucleus and the different suppression factors for ${}^{6,7}_{3}Li + {}^{152}_{62}Sm$ reactions occur as a consequence of the different nuclear structure of the projectiles. The breakup threshold of the projectile $\left({}^{7}_{3}Li\right)$ is *2.45* MeV and is larger than that of the ${}^{6}_{3}Li$ -projectile (*BE = 1.475* MeV), and thus, the effects of the breakup channel are more pronounced in the fusion dynamics of ${}^{6}_{3}Li + {}^{152}_{62}Sm$ reaction in comparison to that of ${}^{7}_{3}Li + {}^{152}_{62}Sm$ reaction. The projectile $\left({}^{7}_{3}Li\right)$ can be taken as two body $a + t$ cluster structure with a breakup threshold of 2.45*MeV*. Rath et al. [33] pointed out that the above barrier complete fusion data of this reaction is reduced by 25% with reference to the expectations coupled channel calculations. The projectile $\left({}^{7}_{3}Li\right)$ possesses quadrupole moment ($Q_m = -4.06\ \mathrm{fm}^2$) in its ground state along with the bound first excited state $\left(\frac{1^-}{2}, 0.4776\ \mathrm{MeV}\right)$. The transition probability ($B(E2\uparrow)$) is equals to $8.30\ e^2\ \mathrm{fm}^4$ from first excited state to the ground state [33]. The coupling of the projectile degrees of freedom and rotational states up to $10^+$ ground state rotational band having $\beta_2 = 0.280$ and $\beta_4 = 0.005$ for ${}^{152}_{62}Sm$ nucleus are capable of reproducing the sub-barrier fusion enhancement of ${}^{7}_{3}Li + {}^{152}_{62}Sm$ reaction, but it leads to the over predictions to the complete fusion data at above barrier energies. Thus, the above barrier complete fusion data of ${}^{7}_{3}Li + {}^{152}_{62}Sm$ reaction is suppressed by 25% with respect to the coupled channel description as inferred from the Fig. 6b.

In spite of this, the EDWSP model calculations properly accounted the sub-barrier fusion data. Although the complete fusion data in above barrier energy regions is also inhibited with respect to the expectations of the EDWSP model, the large discrepancies between the coupled channel calculations and the above barrier complete fusion data can be minimized up to 13% (8%) for ${}^{6}_{3}Li + {}^{152}_{62}Sm\left({}^{7}_{3}Li + {}^{152}_{62}Sm\right)$ reaction as depicted in Fig. 6. This fusion suppression can be correlated with the breakup of the projectile due to its low binding energy. In the vicinity of target field, the projectile breakup before reaching the Coulomb barrier and hence displays a strong impression of the breakup channel on the tunneling probability as well as the fusion cross sections. It is well recognized that the channel coupling effects impart negligible influence to the complete fusion data in above barrier energy region; henceforth, the overestimations of the coupled channel calculations to data reflect the shifting of the fusion flux into other reaction channels and thus maintains the suppression of the complete fusion data in above barrier energy regions. The EDWSP model calculations estimate the suppression factor up to 15% (17%) for ${}^{6}_{3}Li + {}^{152}_{62}Sm\left({}^{7}_{3}Li + {}^{152}_{62}Sm\right)$ reaction. The extracted fusion suppression factor is smaller by 13% (8%) for ${}^{6}_{3}Li + {}^{152}_{62}Sm\left({}^{7}_{3}Li + {}^{152}_{62}Sm\right)$ reaction with respect to the reported values [31–33] as depicted in Fig. 6.

### 3.1 $\chi^2$ Analysis of the Fusion Data

For fusion excitation function, the goodness of fit of a given model calculations can be judged by $\chi^2$ analysis which can be obtained by using following relation [5, 76].

$$\chi^2 = \frac{1}{N}\sum_{i=1}^{N}\left[\frac{\left\{\sigma_{\mathrm{Exp}}(E_i) - \sigma_{Model}(E_i)\right\}^2}{\sigma_{Model}(E_i)}\right]$$

where, $N$ are the number of points, $E_i$ are the experimental energies, $\sigma_{\mathrm{Exp}}$ and $\sigma_{\mathrm{Model}}$ are the experimental and model cross sections, respectively. $\chi^2$ measures the deviation of theoretical predictions from the experimentally observed data, and therefore, $\chi^2$ analysis has been done for EDWSP model calculations in above barrier energy region for ${}^{6,7}_{3}Li + {}^{152}_{62}Sm$ reactions. The values of $\chi^2$ per degrees of freedom obtained under present model calculations are $\chi^2 = 2.25$ for ${}^{6}_{3}Li + {}^{152}_{62}Sm$ reaction and $\chi^2 = 1.80$ for ${}^{7}_{3}Li + {}^{152}_{62}Sm$ reaction. For ${}^{16}_{8}O + {}^{144,148,150,152,154}_{62}Sm$ reactions, $\chi^2$ analysis have been obtained for EDWSP model calculations predictions of fusion cross sections. The $\chi^2$ values for the spherical choice of projectile-target combinations such as ${}^{16}_{8}O + {}^{144}_{62}Sm$ and ${}^{16}_{8}O + {}^{148}_{62}Sm$ reactions are 1.92 and 2.25, respectively. For deformed nuclei, the $\chi^2$ values are 2.82, 3.08, and 1.98 for ${}^{16}_{8}O + {}^{150}_{62}Sm$, ${}^{16}_{8}O + {}^{152}_{62}Sm$, and ${}^{16}_{8}O + {}^{154}_{62}Sm$ reaction, respectively. The minimum $\chi^2$ values obtained for abovementioned reactions suggest that the predictions of the EDWSP model are adequate for ${}^{6}_{3}Li + {}^{152}_{62}Sm\left({}^{7}_{3}Li + {}^{152}_{62}Sm\right)$ reaction, and hence, the fusion suppression at above barrier energies is 15% (17%) with reference to the EDWSP model calculations. In other words, the present model calculations provide a fine tuning that produces a better $\chi^2$ fit to the experimental fusion data.

In below-barrier regions, the close agreement between theoretical predictions and the fusion data can be easily observed in Fig. 6. However, to highlight the agreement between theoretical results and above barrier complete fusion data, the fusion excitation functions of ${}^{6,7}_{3}Li + {}^{152}_{62}Sm$ reactions (theoretical calculations and fusion data) are shown in linear scale [Fig. 7]. At above barrier energies, the theoretical results of coupled channel approach (with and without internal structure degrees of freedom) merge each other. The EDWSP model calculations, with a suppression factor of 15% (17%) for ${}^{6}_{3}Li + {}^{152}_{62}Sm\left({}^{7}_{3}Li + {}^{152}_{62}Sm\right)$ reaction, provide the close agreement with the above barrier complete fusion data. This clearly suggest that the intrinsic degrees of freedom associated with the colliding pairs offers negligible influence on fusion cross sections at above barrier energies while the sub-barrier fusion

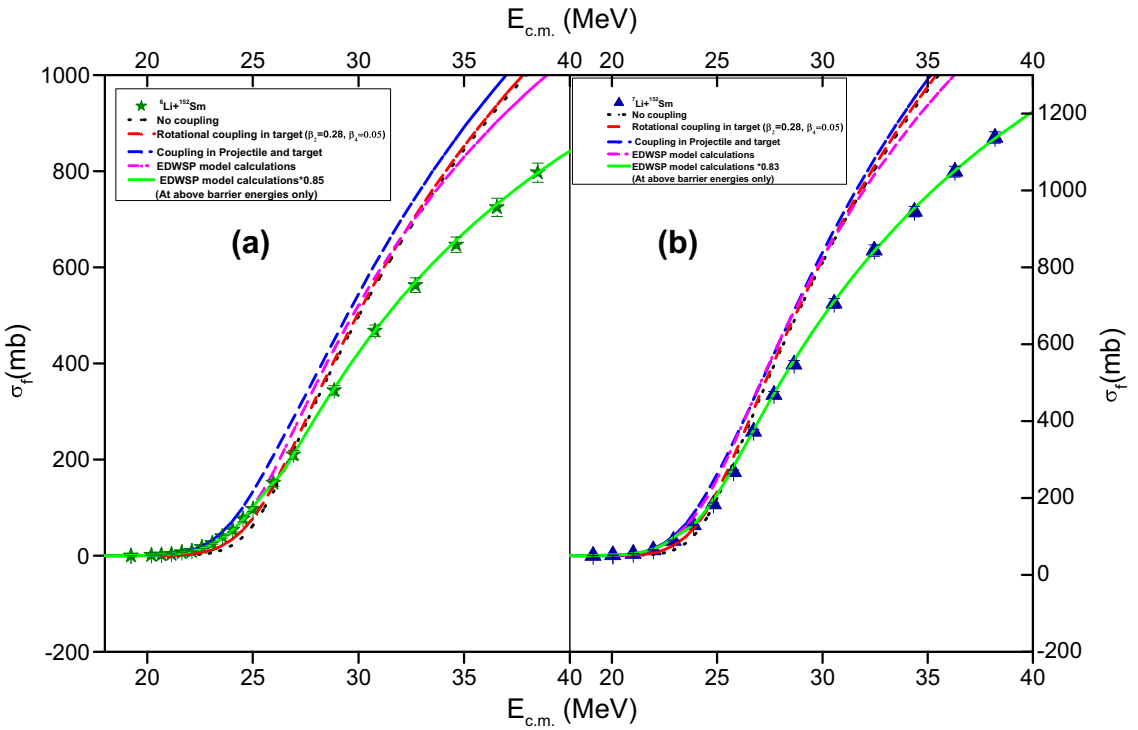


**Fig. 7** Same as in Fig. 6, but in linear scale

excitation functions are quite sensitive to the addition of the intrinsic channels of collision partners.

## 4 Conclusions

We have analyzed the fusion dynamics of ${}^{16}_{8}O + {}^{144,148,150,152,154}_{62}Sm$ and ${}^{6,7}_{3}Li + {}^{152}_{62}Sm$ reactions within the coupled channel approach and the EDWSP model. In the case of ${}^{16}_{8}O + {}^{144,148,150,152,154}_{62}Sm$, the target isotopes exhibit a structural change from spherical symmetry to a statically deformed shape and consequently the dominance of rotational couplings over vibrational couplings, which increases with the neutron richness of the target. For the lightest targets $\left({}^{144,148}_{62}Sm\right)$, the collective excitations of the colliding pairs are the dominant mode of couplings, while for the heaviest isotopes $\left({}^{150,152,154}_{62}Sm\right)$, the rotational states play a major role in the fusion enhancement at sub - barrier energies. The larger sub-barrier fusion enhancement of the ${}^{16}_{8}O + {}^{150,152,154}_{62}Sm$ systems in reference to the ${}^{16}_{8}O + {}^{144,148}_{62}Sm$ systems can be correlated with the dominance of static deformations over the inelastic surface excitations associated with the target nuclei.

In contrast, complete fusion data at above - barrier energies for ${}^{6,7}_{3}Li + {}^{152}_{62}Sm$ reactions were found to be lowered considerably when compared with the predictions of the theoretical approaches (coupled channel approach and EDWSP model). Within the view of the EDWSP model, the extracted fusion suppression effects at above - barrier energies can be estimated to be 15% (17%) for ${}^{6}_{3}Li + {}^{152}_{62}Sm\left({}^{7}_{3}Li + {}^{152}_{62}Sm\right)$ reaction, which are smaller than those predicted in literature by 13% (8%) for ${}^{6}_{3}Li + {}^{152}_{62}Sm\left({}^{7}_{3}Li + {}^{152}_{62}Sm\right)$ reaction. Such suppression effects can be correlated with the low breakup threshold of *alpha*-breakup channel associated with weakly bound system. The projectiles $\left({}^{6,7}_{3}Li\right)$ are loosely bound nuclei due to their low breakup threshold, which, in turn, breakup before reaching the fusion barrier and, henceforth, automatically regulates the suppression of the complete fusion data at above barrier energies. Further, the observed suppression effects suggest that greater barrier modifications occur for more weakly bound system.

## References

1. A.O. Caldeira, A.J. Leggett, Phys. Rev. Lett. **46**, 211 (1981)
2. J.D. Bierman et al., Phys. Rev. Lett. **76**, 1587 (1996)
3. M.S. Gautam, Indian J. Phys. **90**, 335 (2016)
4. P.R.S. Gomes et al., Phys. Rev. C **49**, 245 (1994)
5. E.F. Aguilera et al., Phys. Rev. C **52**, 3103 (1995)
6. J.R. Leigh et al., Phys. Rev. C **52**, 3151 (1995)

7. M.S. Gautam, Nucl. Phys. A **933**, 272 (2015)
8. A.A. Sonzogni et al., Phys. Rev. C **57**, 722 (1998)
9. N.V.S.V. Prasad et al., Nucl. Phys. A **603**, 176 (1996)
10. H.Q. Zhang et al., Phys. Rev. C **82**, 054609 (2010)
11. M.S. Gautam, Phys. Scr. **90**, 055301 (2015)
12. C.H. Dasso et al., Nucl. Phys. A **405**, 381 (1983)
13. J.X. Wei et al., Phys. Rev. Lett. **67**, 3368 (1991)
14. C.R. Morton et al., Phys. Rev. Lett. **72**, 4074 (1994)
15. M.S. Gautam, Mod. Phys. Lett. A **30**, 1550013 (2015)
16. L.F. Canto et al., Phys. Rep. **424**, 1 (2006)
17. K. Hagino, N. Takigawa, Prog. Theor. Phys. **128**, 1061 (2012)
18. A.M. Stefanini et al., Phys. Rev. C **62**, 014601 (2000)
19. V. Tripathi et al., Phys. Rev. C **65**, 014614 (2001)
20. M.S. Gautam et al., Phys. Rev. C **92**, 054605 (2015)
21. A.M. Stefanini et al., Phys. Rev. C **73**, 034606 (2006)
22. R.G. Stokstad et al., Phys. Rev. C **23**, 281 (1981)
23. R.G. Stokstad et al., Phys. Rev. C **21**, 2427 (1980)
24. H. Esbensen, Nucl. Phys. A **352**, 147 (1981)
25. W. Reisdorf et al., Nucl. Phys. A **438**, 212 (1985)
26. W. Reisdorf et al., Phys. Rev. Lett. **49**, 1811 (1982)
27. N. Rowley et al., Phys. Lett. B **254**, 25 (1991)
28. K. Hagino, N. Rowley, A.T. Kruppa, Comput. Phys. Commun. **123**, 143 (1999) K Hagino (private communication)
29. M.S. Sukhvinder, R. Kharab, Nucl. Phys. A **897**, 179 (2013)
30. M.S. Gautam, Phys. Rev. C **90**, 024620 (2014)
31. P.K. Rath et al., Phys. Rev. C **79**, 051601 (2009)
32. P.K. Rath et al., Nucl. Phys. A **874**, 14 (2012)
33. P.K. Rath et al., Phys. Rev. C **88**, 044617 (2013)
34. Z.H. Liu et al., Eur. Phys. J. A **26**, 73 (2005)
35. M.S. Hussein et al., Phys. Rev. C **46**, 377 (1992)
36. M.S. Hussein et al., Phys. Rev. C **51**, 846 (1995)
37. M.S. Gautam, Can. J. Phys. **93**, 1343 (2015)
38. C.H. Dasso et al., Phys. Rev. C **50**, R12 (1994)
39. C.H. Dasso et al., Phys. Lett. B **276**, 1 (1992)
40. K.E. Zyromski et al., Phys. Rev. C **55**, R562 (1997)
41. P.A. DeYong et al., Phys. Rev. C **58**, 3442 (1998)
42. J.J. Kolata et al., Phys. Rev. Lett. **81**, 4580 (1998)
43. M. Trotta et al., Phys. Rev. Lett. **84**, 2342 (2000)
44. M. Dasgupta et al., Phys. Rev. Lett. **82**, 1395 (1999)
45. C. Signorini et al., Eur. Phys. J. A **5**, 7 (1999)
46. M. Dasgupta et al., Phys. Rev. C **66**, 041602(R) (2002)
47. V. Tripathi et al., Phys. Rev. Lett. **88**, 172701 (2002)
48. H. Kumawat et al., Phys. Rev. C **86**, 024607 (2012)
49. D.L. Hill, J.A. Wheeler, Phys. Rev. **89**, 1102 (1953)
50. C.Y. Wong, Phys. Rev. Lett. **31**, 766 (1973)
51. M.S. Sukhvinder, R. Kharab, Nucl. Phys. A **897**, 198 (2013)
52. J.O. Newton et al., Phys. Rev. C **70**, 024605 (2004)
53. A. Mukherjee et al., Phys. Rev. C **75**, 044608 (2007)
54. L.C. Chamon et al., Phys. Rev. C **66**, 014610 (2002)
55. K. Washiyama, D. Lacroix, Phys. Rev. C **74**, 024610 (2008)
56. A.S. Umar, C. Simenel, V.E. Oberacker, Phys. Rev. C **89**, 034611 (2011)
57. A.S. Umar, V.E. Oberacker, Eur. Phys. J. A **39**, 243 (2009)
58. E.F. Aguilera, J.J. Kolata, Phys. Rev. C **85**, 014603 (2012)
59. K. Hagino et al., J. Phys. G **23**, 1413 (1997)
60. V.I. Zagrebaev, V.V. Samarin, Phys. At. Nucl. **67**, 1488 (2004)
61. R.A. Gatenby et al., Phys. Rev. C **41**, R414 (1990)
62. R.A. Gatenby et al., Phys. Rev. C **56**, 633 (1993)
63. N. Takigawa et al., J. Phys. G **23**, 1367 (1997)
64. K. Hagino et al., Phys. Rev. C **57**, 1349 (1997)
65. D.E. DiGregorio et al., Phys. Rev. C **39**, 516 (1989)
66. I.J. Thompson, Com. Phys. Report **7**, 167 (1988)
67. A. Diaz-Torres, I.J. Thompson, Phys. Rev. C **65**, 024606 (2002)
68. P.R.S. Gomes et al., Journal of Physics G (Conferences Series) **420**, 012121 (2013)
69. C. Signorini et al., Phys. Rev. C **67**, 044607 (2003)
70. D.R. Otomar et al., Eur. Phys. J. A **46**, 285 (2010)
71. D.R. Otomar et al., Phys. Rev. C **87**, 014615 (2013)
72. D.H. Luong et al., Phys. Lett. B **695**, 105 (2011)
73. M. Dasgupta et al., Nucl. Phys. A **834**, 147c (2010)
74. R. Rafiei et al., Phys. Rev. C **81**, 024601 (2010)
75. N.A. Elmahdy et al., Eur. Phys. J. A **51**, 62 (2015)
76. E.F. Aguilera et al., Phys. Rev. C **41**, 910 (1990)